

Learnable Weight Initialization for Volumetric Medical Image Segmentation

Shahina Kunhimon, Abdelrahman Shaker, Muzammal Naseer, Salman Khan, Fahad Shahbaz Khan

Abstract—Hybrid volumetric medical image segmentation models, combining the advantages of local convolution and global attention, have recently received considerable attention. While mainly focusing on architectural modifications, most existing hybrid approaches still use conventional data-independent weight initialization schemes which restrict their performance due to ignoring the inherent volumetric nature of the medical data. To address this issue, we propose a learnable weight initialization approach that utilizes the available medical training data to effectively learn the contextual and structural cues via the proposed self-supervised objectives. Our approach is easy to integrate into any hybrid model and requires no external training data. Experiments on multi-organ and lung cancer segmentation tasks demonstrate the effectiveness of our approach, leading to state-of-the-art segmentation performance. Our proposed data-dependent initialization approach performs favorably as compared to the SwinUNETR model pretrained using large-scale datasets on multi-organ segmentation task. Our source code and models are available at: <https://github.com/ShahinaKK/LWI-VMS>.

Index Terms—Hybrid architecture, Volumetric medical segmentation, Weight initialization.

I. INTRODUCTION

In medical image segmentation, target organs and tissues are pixel-wise classified, enabling better diagnosis, and treatment planning. Advances in deep learning methods have significantly improved medical image segmentation tasks, such as tumor segmentation [1], [2] and lesion segmentation [3]. Various successful convolutional neural network (CNN) models, self attention (SA) based transformer models and their combinations have been adapted for medical image segmentation tasks. Generally, it is necessary to have a large amount of annotated training data in order to achieve promising results with deep neural networks [4]. However, it is a complex and expensive process to collect and annotate medical images to curate large-scale benchmark datasets. The ethical and legal constraints associated with the medical data to preserve the privacy and security of sensitive patient information makes the data collection and annotation task more challenging. Therefore,

majority of the existing medical image segmentation methods focus on improving the architecture of deep neural networks. The recent developments in vision transformers (ViTs) [4]–[6] have enabled a hybrid design [1], [7] incorporating the complementary properties of convolutional networks and self-attention based vision transformers for volumetric medical segmentation. However, we observe that these hybrid CNN-transformer models are typically initialized using conventional and *data-independent* weight initialization schemes [8], [9], which can affect their overall segmentation performance. For example, the model training can converge to different solutions based on the weight initialization scheme as discussed in Section III-A.

In this work, we argue that self-supervised inductive biases which strive to capture the nature of volumetric data are likely to perform better than the conventional weight initialization schemes that are independent of data. To this end, we propose a *learnable weight initialization* approach that strives to explicitly exploit the volumetric nature of the medical data to induce contextual cues within the model at the early stage of the training. These contextual cues are learned using our proposed self-supervised objectives. The segmentation models are based on encoder-decoder network design. Therefore, to learn contextual cues from a given volumetric input, our approach encourages the encoder to predict the correct order of shuffled sub-volumes while training the decoder to reconstruct the masked organs or part of an organ (Sec.III-B). As a result, data-dependent priors about the input structure can be effectively captured within the model weights across different scans of the volumetric input, resulting in better segmentation performance. Our contributions are as follows:

- We propose a learnable weight initialization method that can be integrated into any hybrid volumetric medical segmentation model to effectively train small-scale datasets.
- To learn such a weight initialization, we propose data-dependent self-supervised objectives tailored to learn the structural and contextual cues from the volumetric medical image datasets.
- We demonstrate the effectiveness of our approach by conducting experiments for multi-organ and tumor segmentation tasks, achieving superior segmentation performance without requiring additional external training data.
- Our proposed weight initialization scheme, which relies solely on the training dataset at hand yields favorable results when compared to the single model performance

This manuscript was submitted on 26/06/2023

Shahina Kunhimon is with the Department of Machine Learning, Mohammed Bin Zayed University of Artificial Intelligence (MBZUAI), Abu Dhabi, UAE (e-mail: shahina.kunhimon@mbzuai.ac.ae).

Abdelrahman Shaker, Dr Muzammal Naseer, Dr Salman Khan are with Mohammed Bin Zayed University of Artificial Intelligence, UAE.

Dr Fahad Shahbaz Khan is with Mohammed Bin Zayed University of Artificial Intelligence, UAE and Linkoping University, Sweden.

of Swin-UNETR large-scale self supervised pretraining [10] on synapse multi-organ segmentation task.

II. RELATED WORK

Medical image segmentation using deep learning techniques has garnered significant interest in healthcare research. These techniques can be broadly categorized into three groups: CNN based, transformer based and hybrid approaches.

A. CNN-based Methods

A variety of models incorporating encoder-decoder structures with diverse CNN backbones have been adopted for medical image segmentation tasks. Fully Convolutional Networks (FCN) [11], Deeplab [12], U-Net [13] were some of them. Since the introduction of U-Net, various CNN-based approaches [14]–[18] have been introduced to extend the typical 2D U-Net architecture for different 2D as well as 3D medical image segmentation tasks. Feature extraction using 2D slices is not considered optimal for volumetric 3D medical image segmentation as it completely discards the crucial low-level information in one axis.

In order to overcome this drawback, significant number of 3D approaches which directly utilizes the volumetric images were introduced. V-Net is a hierarchical framework introduced in [19] directly utilizes the 3D representations and preserves the relevant image features by down-sampling the volume to lower resolutions. 3D U-Net proposed in [20] is a 3D-extension of U-Net which directly operates on 3D representations by substituting the 2D operations with their respective 3D counterparts. A generic segmentation framework called nnUNet designed to automatically configure the optimal data preprocessing steps and model architecture based on the data characteristics was introduced in [21]. [22] proposed a multi-scale framework designed to learn image representations from different resolutions using a 3D fully convolutional network for multi-organ segmentation.

However, these CNN based models lack the ability to capture long range correlations in the data due to the intrinsic locality of convolution operations which limits their performance in challenging segmentation problems.

B. Transformer-based Methods

Due to the success of the vision transformer models (ViTs) across various computer vision tasks, recent works have focused on investigating their applicability to medical segmentation tasks. For volumetric medical image segmentation task, pure-transformer based designs were explored in [2] and [23]. In [23], a given volumetric image is divided into 3D patches followed by flattening them to 1D embeddings for learning global representations. Swin-unet introduced in [2] is a pure transformer extension of U-Net which takes 2D image slices as input and makes use of shifted window transformer architecture for segmentation.

Despite having the capability to capture the global structure via self attention, ViTs require pre-training on large-scale datasets to inherent inductive biases and achieve promising performance, thereby limiting their adoption in medical imaging datasets because of the scarcity of the data.

C. Hybrid Methods

Apart from pure CNN or transformer-based designs, an alternative approach that combines the strengths of both CNN and transformer architectures is investigated extensively in recent years. Several recent methods such as [1], [7], [24]–[30] follow this hybrid approach to leverage the spatial awareness of CNNs and the long-range dependency modeling capabilities of transformers.

TransUNet [24] combines the U-Net architecture with a transformer in the expansion path where the output of the convolutional part are flattened into 2D patches and fed to the vision transformer followed by the decoder and the skip connections to concatenate the upsampled encoded features with high-resolution features from the CNN layers to achieve better localization. TransBTS [30] is a 3D extension of TransUNet in which 3D CNN downsamples the image and extracts the local contextual representations followed by the transformer to model global features. In MedT model proposed in [27], a gated position-sensitive axial-attention mechanism is integrated into the self-attention module of the encoder to manage the positional embedding information while the ConvNet module in the decoder part generates a segmentation model. TransFuse is another popular hybrid model introduced in [26] which involves a parallel CNN-transformer architecture with an additional BiFusion module in the encoder to facilitate the fusion of features from multiple levels. Ds-transunet [25] relies on a dual-scale encoder based on Swin transformer [31] to effectively deal with multi-scale inputs and to encode both local as well as global feature representations. UNETR [7] is a hybrid method for 3D medical segmentation tasks and composes of a “U-shaped” encoder-decoder architecture, with a transformer encoder to encode enriched global representation and a convolutional decoder. nnFormer [29] is a combination of interleaved convolution and self-attention operations. Here, local and global volume-based self-attention mechanisms are proposed to encode the volume representations. Recently, UNETR++ [28] extend the architecture of UNETR by replacing the fixed transformer representation of UNETR with a hierarchical efficient paired attention module to reduce the complexity significantly, with higher-quality segmentation masks.

D. Weight Initialization schemes

Weight initialization plays a crucial role in deep neural network training, as it can have strong impact on the training time as well as the quality of the resulting model. The objective of an initializer is to determine the initial network parameter values within a suitable region of optimization landscape so that the training converges to a good solution [32]. Random initialization is the most commonly used approach where the initial weights are assigned by randomly sampling from a given distribution such as standard normal and uniform distributions. In another method called truncated normal, the initial weights are sampled from a normal distribution, similar to standard normal initialization but if the values fall are outside a given range, they are truncated and resampled to be within the limit. Compared to the standard normal method,

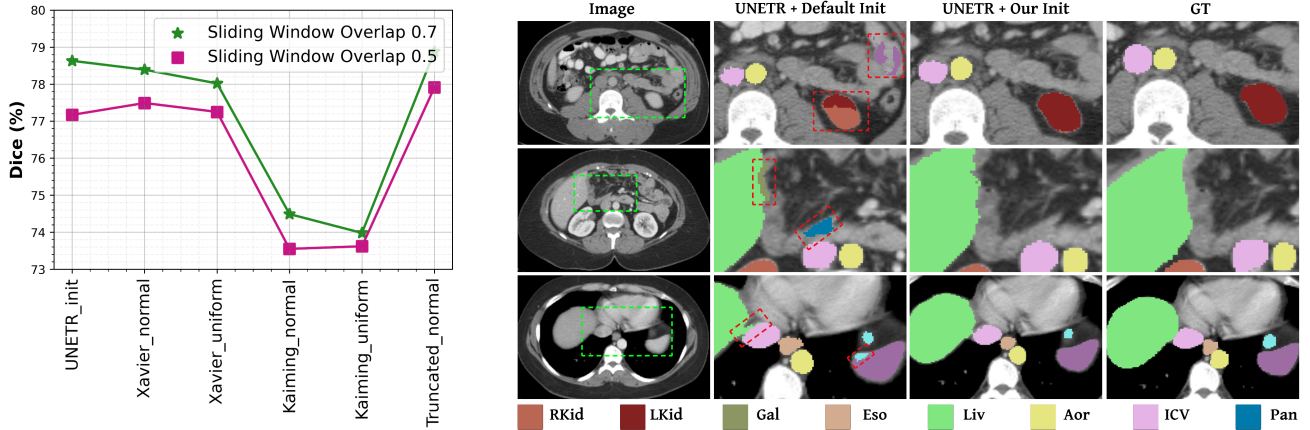


Fig. 1. **Left:** UNETR [7] is sensitive to different data-independent weight initialization schemes. We observe that UNETR performance drops significantly when initialized with the Kaiming normal method. Further, the truncated normal method gives better results than the default UNETR initialization. **Right:** Qualitative comparison on Synapse between the default and our proposed initialization (Init) method within the same UNETR framework. We enlarge the segmented area (green dashed boxes in first column box in column 1). Our method reduces the *false positives* for organs compared to standard UNETR (red dashed box). Organs are shown in the legend below the examples. Best Viewed zoomed in.

this approach provides improved control over the initialization range, which is beneficial when considering prior knowledge or domain specific constraints regarding acceptable range of parameter values. Xavier initialization introduced in [8], also known as Glorot initialization, initializes the weights by sampling from a uniform or normal distribution with its standard deviation dependent on the number of input and output connections. This technique focuses on keeping the variance of the activations and gradients relatively constant during forward and backward propagation. In Xavier uniform method, the range of the values for weight initialization is calculated using a uniform distribution $\mathcal{U}(-a, a)$, where the range limit a is given by:

$$a = 6 * \sqrt{\frac{2}{c_{in} + c_{out}}} \quad (1)$$

For the Xavier initialization method using normal distribution $\mathcal{N}(0, \sigma^2)$, the standard deviation σ is given by:

$$\sigma = G * \sqrt{\frac{2}{c_{in} + c_{out}}} \quad (2)$$

In equations 1 and 2, G corresponds to an optional scaling factor and c_{in} and c_{out} represents the number of previous layer (input) and current layer (output) connections respectively. Kaiming He Initialization [9] is a variant of Xavier initialization introduced to mitigate the issue of vanishing gradients associated with the non linear activations by adjusting the distribution based on the number of inputs to the current layer. In Kaiming uniform method, the values for weight initialization is based on a uniform distribution $\mathcal{U}(-b, b)$ bounded by the limit b which is given by:

$$b = G * \sqrt{\frac{3}{c_{in}}} \quad (3)$$

For the Kaiming initialization method using normal distribution $\mathcal{N}(0, \sigma^2)$, the standard deviation σ is given by:

$$\sigma = \frac{G}{\sqrt{c_{in}}} \quad (4)$$

G corresponds to an optional scaling factor and c_{in} represents the number of input connections.

Mostly, the general data-independent weight initialization techniques are adopted for medical imaging tasks. But, medical image datasets are very different from the natural image dataset with respect to the variabilities in terms of imaging modalities and anatomical structure. Also, the class imbalance issues are very prominent in medical imaging segmentation datasets as the region of interest (tumors or any structural abnormality) is relatively rare compared to the background or normal regions in the image. Hence, specific data-dependent weight initialization schemes tailored for medical image segmentation task can guide the model to learn more meaningful representations by incorporating the prior knowledge about the variability in the imaging modalities and object anatomy, reducing the bias towards dominant classes and thereby improve the segmentation outcome. Pretraining on large scale datasets is a popular data-dependent initialization approach explored across various application fields of deep learning. For volumetric medical image segmentation, pretraining on large-scale natural image datasets cannot guarantee good generalization due to the difference in the image distribution. Large scale pretraining on medical datasets is not favourable since annotated medical data is deficient. Although self supervised pretraining approaches introduced in [10], [33] were proven to be effective for volumetric segmentation, these methods heavily depend on large-scale medical datasets, which consequently contributes to increased data and computational costs.

In this work, we propose a learnable weight initialization scheme that utilizes limited data to learn discriminative characteristics from the volumetric medical images, which can improve the model performance without the need of additional data or higher computation costs.

III. METHOD

A. Data Independent Weight Initialization

As discussed earlier, deep neural networks (DNNs) typically require a large amount of training data to achieve promis-

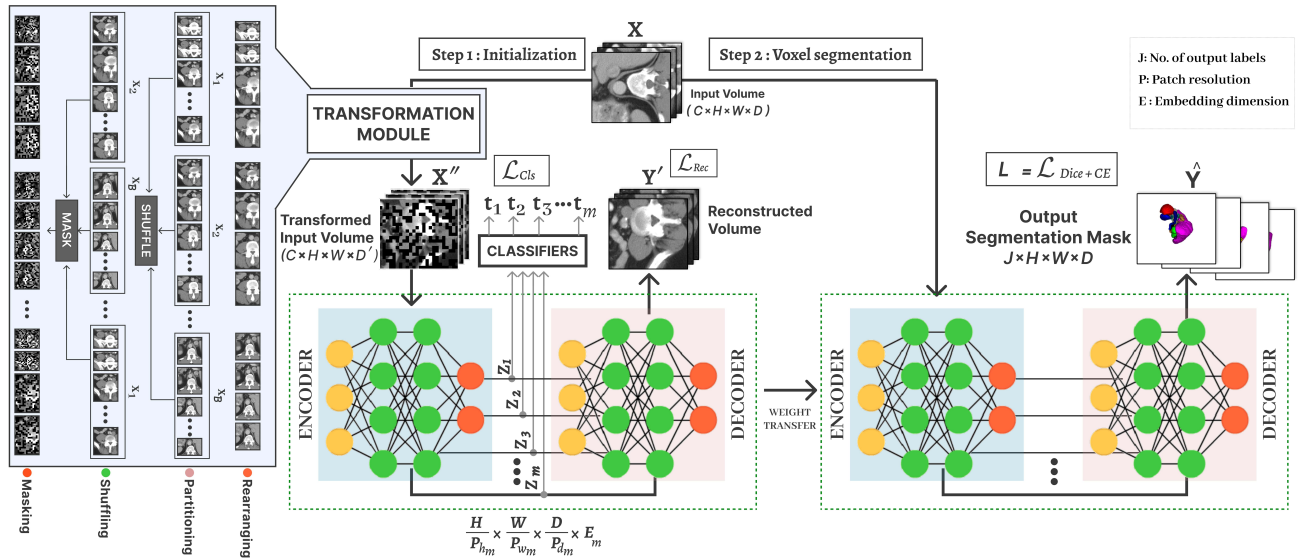


Fig. 2. Overview of our proposed approach: To learn weight initialization using self-supervised tasks defined by the volumetric nature of the medical data. In the early stage of training (Step-1), we define the order prediction task within the encoder latent space, while simultaneously the decoder has to reconstruct the missing organs from masked&shuffled input. The masked&shuffled input is the result of our transformation module with 4 stages: depth wise rearranging, partitioning into equal size sub-volumes, random shuffling of sub-volumes for the order prediction objective, and finally masking shuffled volume for the reconstruction objective. This allows the model to learn structural and contextual consistency about the data that provides an effective initialization for segmentation task (Step-2). Our approach does not rely on any extra data and therefore remains as computationally effective as the baseline while enhancing the segmentation performance.

ing results. However, this is challenging in medical imaging tasks due to the scarcity of ample medical training data. Collecting and annotating medical images is a complex and expensive process. This becomes further problematic in case of transformers-based medical segmentation approaches due to the lack of inductive biases, thereby requiring a large amount of training data. Most existing medical image segmentation methods [1], [7], [28]–[30] address this issue by focusing on architectural improvements, such as integrating CNNs with ViTs to inherit the inductive biases, or using hierarchical structural representations. These hybrid CNN-transformers approaches typically strive to improve the locality of ViTs. However, they mostly utilize the standard *data-independent* initialization schemes such as truncated normal, Xavier [8], and Kaiming He [9], which do not explicitly take into account the volumetric characteristics of the medical segmentation data. For instance, the default weight initialization scheme in the UNETR framework [7] is

$$\begin{cases} \mathcal{U}(-\sqrt{\sigma}, \sqrt{\sigma}), \sigma = \frac{1}{C * \prod_{i=0}^2 ksize(i)}; & \text{Convolutional Layers} \\ \mathcal{U}(-\sqrt{\sigma}, \sqrt{\sigma}), \sigma = \frac{1}{C}; & \text{Linear Layers} \end{cases} \quad (5)$$

Where \mathcal{U} is a continuous uniform distribution, σ is the standard deviation, C is the number of input channels, and $ksize$ is the kernel size at position i .

We observe that the choice of the initialization scheme plays an important role in network learning and can affect the model convergence. For instance, Fig. 1 (left) shows that UNETR [7] converges to different solutions based on the model initialization. Using data-independent initialization can likely limit the performance as medical segmentation datasets have fewer samples than the large-scale natural image

benchmarks. Therefore, the model may struggle to learn the representations effectively during the training process, when the number of training samples is relatively lower with respect to the network parameters.

In this work, we propose a *data-dependent learnable weight initialization* method that explicitly takes into account the volumetric nature of the medical data. Our approach induces structural and contextual consistency within encoder-decoder networks in the early stage of the training, leading to improved segmentation performance (e.g., fewer false positives and better delineation of segmentation boundaries) as shown in Fig. 1 (right). The useful prior knowledge about data-dependent biases learned by our approach provides a better starting point for model training that leads to improved segmentation without utilizing additional data or increasing the computation costs.

B. Learning Data-Dependent Weight Initialization

Our work focuses on designing a learnable weight initialization method for hybrid volumetric medical image segmentation frameworks. Consider a hybrid volumetric medical image segmentation network that consists of a ViT encoder \mathcal{F} and a CNN-based decoder \mathcal{G} . The encoder converts 3D input patches into latent feature representations \mathbf{Z}_i at multiple levels i . The output segmentation mask (\hat{Y}) is generated by combining encoder representations at multiple resolutions with the corresponding upsampled decoder representations. Given a 3D input volume $\mathbf{X} \in \mathbb{R}^{C \times H \times W \times D}$, where C, H, W, D represents the number of channels, height, width, and depth of the image respectively, the latent feature representations generated by the encoder can be represented as:

$$\mathcal{F}(\mathbf{X}) = \mathbf{Z}_i \in \mathbb{R}^{\frac{H}{P_{h_i}} \times \frac{W}{P_{w_i}} \times \frac{D}{P_{d_i}} \times E_i}; \quad i = 1, 2, \dots, m \quad (6)$$

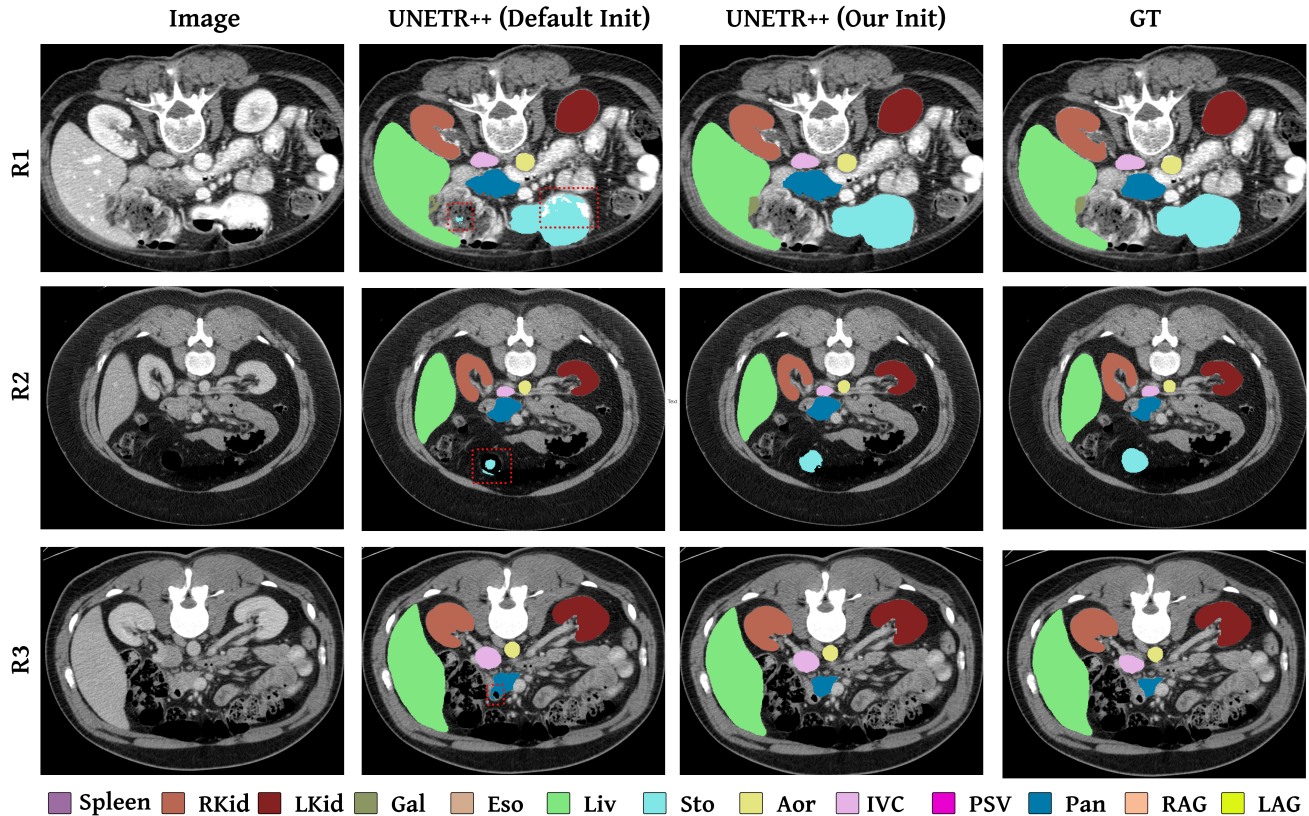


Fig. 3. Qualitative results for multi-organ synapse dataset on UNETR++ framework: UNETR++ with its default initialization struggles to precisely define the organ boundaries (marked in red dashed box). On the other hand, the proposed data-dependent initialization scheme, when integrated with UNETR++, improves the overall segmentation performance by accurately segmenting the organs and delineating organ boundaries. Organs are shown in the legend below the examples. Abbreviations are as follows: Spl: *spleen*, RKid: *right kidney*, LKid: *left kidney*, Gal: *gallbladder*, Eso: *esophagus*, Liv: *liver*, Sto: *stomach*, Aor: *aorta*, IVC: *inferior vena cava*, PSV: *portal and splenic veins*, Pan: *pancreas*, RAG: *right adrenal gland*, and LAG: *left adrenal gland*. *Best Viewed zoomed in.*

where E_i refer to the embedding size, P_{h_i} , P_{w_i} , P_{d_i} , represents the patch resolution of the encoder representations at layer i across height, width, and depth respectively, and m is the total number of encoder layers connected to the decoder via skip connections.

Our proposed method consists of **(Step 1)** learnable weight initialization in which the model is trained on multi-objective self-supervised tasks to effectively capture the inherent data characteristics, followed by the **(Step 2)** supervised training for the volumetric segmentation task.

Our method utilizes the same training dataset for both steps, and is therefore beneficial for 3D medical imaging segmentation tasks on standard benchmarks having limited data samples. Fig. 2 presents an overview of our approach in a standard encoder-decoder 3D medical segmentation framework. We introduce a *Transformation Module* during **Step 1** to generate masked&shuffled input volume and the encoder-decoder is trained to predict the correct order of medical scans while reconstructing the missing portions as described next.

Step 1- Weight Initialization through Self-supervision: Our approach injects structural and contextual consistency within the transformer architecture through the self-supervised objectives. To effectively capture the underlying patterns in the volumetric Computed Tomography (CT) or Magnetic Resonance Imaging (MRI) data, we transform the given input volume \mathbf{X} using our

proposed transformation module (Fig. 2).

Transformation Module: It rearranges the input volume across the depth and then partitions it to \mathcal{B} non-overlapping of equal-size sub-volumes. For a given input volume of depth D , we define it as $\mathcal{B} = \frac{D}{P_{d_m}}$, where P_{d_m} is the patch resolution at the encoder bottleneck (m^{th} level). We first rearrange the input \mathbf{X} into sub-volumes such as, $\mathbf{X} = [\mathbf{x}_1, \mathbf{x}_2, \dots, \mathbf{x}_{\mathcal{B}}]$. These sub-volumes can be rearranged or shuffled in $|\mathcal{B}|!$ permutations. We randomly select a permutation sequence \mathbf{O} out of them and shuffle the sub-volumes to generate \mathbf{X}' .

We then apply random masking to the shuffled volume \mathbf{X}' using a predefined masking ratio and patch size to obtain a masked&shuffled volume \mathbf{X}'' . The masked&shuffled input volume is then processed by the model to learn data structural and contextual consistency.

Structural Consistency through Order Prediction: Our approach mines intrinsic anatomical information from the volumetric scans to bring structural consistency to the transformer encoder by learning to predict the correct order of the transformed shuffled input. This can be formulated as a classification task with \mathcal{B} classes within the encoder latent space. We append a classifier head at the end of each encoder representation \mathbf{Z}_i (Eq. 6). Then, we flatten and average the encoder representation at each layer \mathbf{Z}_i , $\{i = 1, 2, 3, \dots, m\}$ across the height and width dimension to obtain an interme-

TABLE I

BASELINE COMPARISON ON SYNAPSE: OUR APPROACH SIGNIFICANTLY IMPROVES UNETR ON SYNAPSE. SPECIFICALLY, WE OBSERVE LARGE IMPROVEMENTS IN SMALL ORGANS SUCH AS AORTA, GALLBLADDER, AND PANCREAS.

Method	Spleen	Right kidney	Left kidney	Gallbladder	Liver	Stomach	Aorta	Pancreas	Average
UNETR [7]	88.58	80.03	78.87	62.51	95.45	74.44	84.79	52.70	77.17
UNETR (Ours)	86.72	82.86	85.41	65.15	95.56	75.23	88.07	58.85	79.73

TABLE II

SOTA COMPARISON ON SYNAPSE: WE OBSERVE LARGE VARIANCE IN THE PERFORMANCE OF EXISTING METHODS ACROSS DIFFERENT ORGANS. IN COMPARISON, OUR APPROACH CONSISTENTLY PERFORMS BETTER WHILE INCREASING THE OVERALL PERFORMANCE.

Method	Spleen	Right kidney	Left kidney	Gallbladder	Liver	Stomach	Aorta	Pancreas	Average
U-Net [13]	86.67	68.60	77.77	69.72	93.43	75.58	89.07	53.98	76.85
TransUNet [24]	85.08	77.02	81.87	63.16	94.08	75.62	87.23	55.86	77.49
Swin-UNet [2]	90.66	79.61	83.28	66.53	94.29	76.60	85.47	56.58	79.13
MISSFormer [34]	91.92	82.00	85.21	68.65	94.41	80.81	86.99	65.67	81.96
Swin-UNETR [1]	95.37	86.26	86.99	66.54	95.72	77.01	91.12	68.80	83.48
nnFormer [29]	90.51	86.25	86.57	70.17	96.84	86.83	92.04	83.35	86.57
UNETR++ [28]	95.94	87.16	87.57	68.34	96.35	83.93	92.88	82.16	86.80
UNETR++ (Ours)	95.41	88.92	87.50	73.03	96.24	85.66	92.62	82.55	87.74

diate embedding of size $\mathbb{R}^{\frac{D}{P_{dm}} \times E_i}$. We forward pass these intermediate representations through corresponding classifier to obtain the order prediction $\mathbf{t}_i \in \mathbb{R}^{\frac{D}{P_{dm}} \times \mathcal{B}}$ (see Fig. 2).

We define the structural consistency by predicting the correct order of shuffled input through cross-entropy loss between each output order prediction \mathbf{t}_i and the ground truth permutation used for sub-volume shuffling. Our order prediction loss \mathcal{L}_{Cls} is as follows:

$$\mathcal{L}_{Cls} = \sum_i \sum_{f=1}^{\mathcal{B}} \left(- \sum_{k=1}^{\mathcal{B}} \mathbf{O}_{k,f} \log(\mathbf{t}_i) \right), \quad (7)$$

where $i = 1, 2, 3, \dots, m$ and $f = 1, 2, \dots, \frac{D}{P_{dm}}$.

Here, \mathcal{B} represents the number of classes that corresponds to the number of sub-volumes. $\mathbf{O}_{k,f}$ corresponds to the ground truth order for sub-volume.

Contextual Consistency through Voxel Reconstruction: Our proposed initialization method utilizes 3-dimensional masking and reconstruction task to inject contextual consistency by learning the correspondence between the masked regions and their neighboring context. i.e, the model will be trained to reconstruct the masked volume \mathbf{X}'' at the decoder $\mathbf{Y}' = \mathcal{G}(\mathbf{X}'')$. The reconstruction loss (\mathcal{L}_{Rec}) between the non-masked input \mathbf{X}' and its corresponding reconstructed volume \mathbf{Y}' is measured by voxel-wise mean square error calculated:

$$\mathcal{L}_{Rec} = \mathcal{L}_{MSE}(\mathbf{X}', \mathbf{Y}') = \frac{1}{N} \sum_{n=1}^N (\mathbf{X}'_n - \mathbf{Y}'_n)^2, \quad (8)$$

where, N represents the total number of voxels in the 3D volume. Our final self-supervised training loss \mathcal{L} in the first step is computed as:

$$\mathcal{L} = \mathcal{L}_{Cls} + \mathcal{L}_{Rec} \quad (9)$$

Step II- Training For Segmentation: During the second stage, the model is trained on the same training dataset for segmentation in a supervised fashion by utilizing a combined soft dice and cross-entropy loss [19]. The model weights learned from the first step are transferred to serve as a better initialization for the subsequent segmentation training task. Given an input volume \mathbf{X} and its corresponding ground truth segmentation mask \mathbf{Y} , the model is trained in the second step with the following supervised objective:

$$\mathcal{L} = \mathcal{L}_{Dice+CE}(\mathbf{Y}, \hat{\mathbf{Y}}) \quad (10)$$

where $\hat{\mathbf{Y}}$ is the output segmentation mask produced by the model and the loss function $\mathcal{L}_{Dice+CE}$ is the combination of cross-entropy and soft Dice:

$$\begin{aligned} \mathcal{L}_{Dice+CE}(\mathbf{Y}, \hat{\mathbf{Y}}) = & 1 - \frac{2}{J} \sum_{j=1}^J \frac{\sum_{n=1}^N \mathbf{Y}_{n,j} \hat{\mathbf{Y}}_{n,j}}{\sum_{n=1}^N \mathbf{Y}_{n,j}^2 + \sum_{n=1}^N \hat{\mathbf{Y}}_{n,j}^2} \\ & - \frac{1}{N} \sum_{n=1}^N \sum_{j=1}^J \mathbf{Y}_{n,j} \log \hat{\mathbf{Y}}_{n,j} \end{aligned} \quad (11)$$

where J and N represent the total number of class labels and voxels respectively. $\hat{\mathbf{Y}}_{n,j}$ and $\mathbf{Y}_{n,j}$ denotes the model output and corresponding ground truth probabilities for a class j at a specific voxel n .

C. Generalizability

In contrast to the existing practice of initializing the models with using large-scale natural image dataset (ImageNet) pre-trained weights, or using generic initialization schemes adopted from mainstream computer vision, we transfer the weights learned from the first step to initialize the model training in the second step. The self-supervised inductive

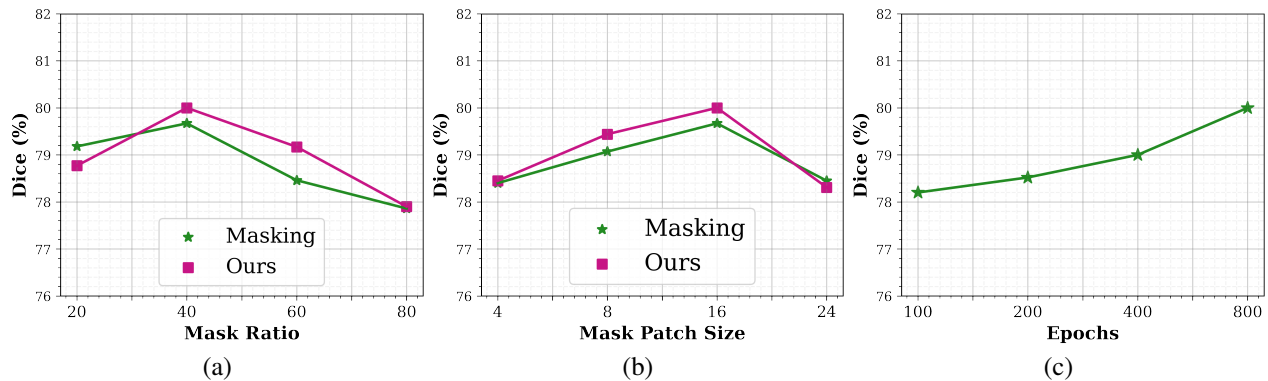


Fig. 4. Effect of masking ratio (a) and mask patch size (b): Moderate masking with masking ratio around 40% and mask patch size of $(16 \times 16 \times 16)$ during the initialization step (step-1) yields the optimal results for UNETR on synapse dataset. **Effect of increasing the training epochs for initialization (c):** Training on our proposed approach on initialization for longer epochs improves the overall segmentation performance.

biases learned during the initialization stage will serve as an effective weight initialization scheme for the subsequent segmentation training task.

Our proposed data-dependent weight initialization approach is complementary and can be integrated into any hybrid volumetric segmentation model to provide a better starting point for model training by learning initial model weights via our proposed self-supervised tasks without modifying the architecture or loss functions. We show that our data-dependent weight initialization scheme performs seamlessly well for both fixed size representation models like UNETR [7] and hierarchical representation models like UNETR++ [28].

IV. RESULTS AND ANALYSIS

A. Datasets

We validate the effectiveness of our proposed approach on two datasets: Synapse for Multi-organ CT Segmentation [35] and Lung dataset from Medical Segmentation Decathlon [36].

Multi-organ Synapse Dataset: Synapse is a CT dataset that consists of abdomen scans of 30 subjects with 8 organs: *spleen, right kidney, left kidney, gallbladder, liver, stomach, aorta and pancreas*. Each CT scan has around 80 to 220 slices with 512×512 pixels. Following the previous approaches, we utilized the data split provided in [24] to train our models on 18 training samples and evaluate on 12 validation cases.

Lung Dataset: Decathlon-Lung dataset from Medical Segmentation Decathlon (MSD) for lung cancer segmentation consists CT volumes of 63 subjects. Lung cancer segmentation is formulated as a binary segmentation task (background or lung cancer). We split the data into 80:20 ratio for training and validation for the experiments.

B. Implementation Details

We implemented our approach in Pytorch and Monai. For fair comparison, we used the same input size and pre-processing steps of UNETR and UNETR++ for our experiments. We train all the models using a single A100 40GB GPU and used sliding window approach with overlap of 0.5 for inference and report the model performance in percentage Dice score (Dice %). All the results are reported based on single model accuracy without any ensemble or additional data.

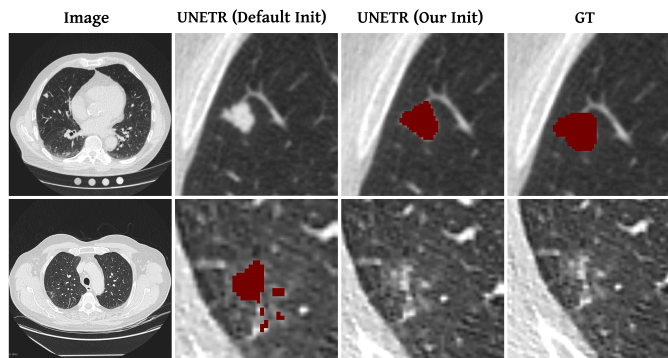


Fig. 5. Qualitative comparison for decathlon lung dataset on UNETR: Integrating our proposed learnable initialization approach is beneficial in learning the structural and contextual cues from the training data which helps in reducing the cases of miss classification (false negatives (row 1) and false positives (row 2)) compared to the UNETR baseline and thereby improves the lung cancer segmentation performance. Best Viewed zoomed in.

C. Baseline Comparison

Table I and Table IV illustrate the impact of our proposed data-dependent initialization approach on the UNETR performance when trained on multi-organ Synapse and Decathlon-Lung datasets. For fair comparison, all the models are trained with input 3D volumes of size $96 \times 96 \times 96$ were used to train the model following the UNETR training framework.

Our approach achieves an absolute gain of 2.56% over the baseline UNETR for Synapse dataset with significant improvement in the segmentation results of smaller organs such as aorta, gallbladder, and pancreas.

For the decathlon-lung dataset, by integrating our proposed weight initialization approach, the lung-cancer segmentation result improved by 1.17% compared to the UNETR baseline as shown in Table IV. It is clear from the Fig. 5 that our approach improves the lung cancer segmentation by reducing the instances of miss classification.

D. State-of-the-Art Comparison

We integrate our approach with the state-of-the-art method UNETR++ on Synapse dataset and achieve an improvement

TABLE III
SOTA COMPARISON: LUNG DATASET

Method	Dice(%)
nnUNet [21]	74.31
Swin UNETR [1]	75.55
nnFormer [29]	77.95
UNETR++ [28]	80.68
UNETR++ (Ours)	81.69

TABLE IV
BASELINE COMPARISON: LUNG DATASET

Model	Dice (%)
UNETR [7]	69.11
UNETR(Ours)	70.28

in the Dice score by 0.94% (Table II). From the organ-wise results shown in the table, we could see that while many existing approaches fails to achieve satisfactory results across different organs, our approach excels by consistently delivering high performance for all organs. As shown in Fig. 3, our approach improves the state-of-the-art on synapse by precisely segmenting the organ boundaries.

For fair comparison, all the experiments on UNETR++ were performed using the same network configuration as shown in Table V. To integrate our proposed method, the models were trained on initialization step for 200 epochs with learning rate $1e-4$ prior to the 1000 epochs of training for segmentation with learning rate 0.01.

The qualitative comparison of Lung dataset segmentation results given in Fig. 6 indicate that our approach helps in reducing the false positives for lung cancer segmentation and thereby improves the Decathlon-Lung state-of-the-art results on UNETR++ by 1.01% as shown in Table III.

E. Ablation Study

Masking Ratio: We evaluated the effect of the masking ratio and mask patch size used in the proposed self-supervised task and we could observe that very small and large patch sizes for masking as well as the masking ratio are not suitable for effective performance (Fig. 4(a),(b)). For an input volume size of $96 \times 96 \times 96$, the experimental results on multi-organ synapse dataset, a masking ratio of 40% and mask patch size of $16 \times 16 \times 16$ during the initialization step results in the best downstream segmentation performance. The optimal

TABLE V
NETWORK CONFIGURATION OF UNETR++

Attribute	Synapse	Lungs
Spacing	[0.76, 0.76, 3]	[1.52, 1.52, 6.35]
Crop size	$(128 \times 128 \times 64)$	$(192 \times 192 \times 32)$
Batch size	2	2

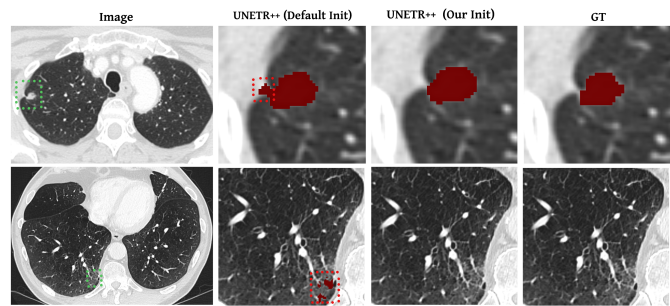


Fig. 6. **Qualitative results (Lungs) on UNETR++:** column 2-4 shows the enlarged views of the segmented areas marked in green dashed box in column 1. Our approach reduces the false positives (marked in red dashed box). Best Viewed zoomed in.

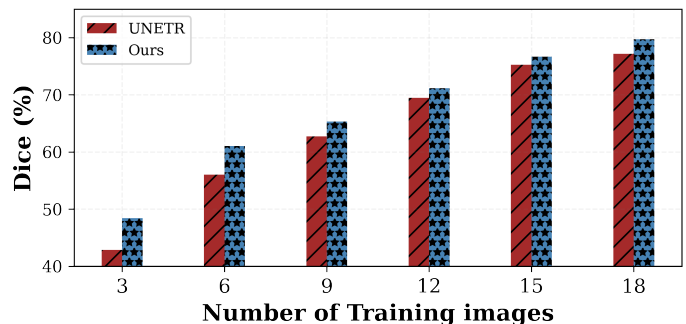


Fig. 7. **Effect of Training data size:** Our approach outperforms the UNETR baseline by high margin when trained with few data examples.

masking ratio and mask patch size may vary based on the network and dataset characteristics since medical images have different modalities and intensity ranges. Hence, they can be considered as hyperparameters which can be tuned using a held-out validation set .

Effect of training epochs: We studied the effect of varying the training period for the initialization step (step-1) on UNETR performance for synapse dataset and the results are illustrated in Fig. 4 (c) . We observed that large number of epochs during step-1 of our approach helps to better capture volumetric data characteristics which in return further increases the performance. We set the number of epochs during Step-1 to 800.

Table VII shows that integrating our data-specific initialization to UNETR without increasing the total training epochs (800 epochs of step-1 and 4200 epochs of step-2) can also improve results while increasing the training epochs (5800 epochs) of UNETR without our initialization does not lead to notable improvements.

Effect of training data size: We evaluated how varying the amount of data available during training impacts the UNETR performance for synapse dataset. The results as shown in Fig. 7 demonstrates that our approach consistently performs better than the UNETR baseline especially with fewer number of training examples. The ability to enhance results in such data-constrained scenarios is particularly valuable, as it helps overcome challenges associated with insufficient data and improves the overall applicability and effectiveness of the segmentation approach.

Comparing different self supervised objectives: The effect

TABLE VI
EFFECT OF DIFFERENT SELF-SUPERVISED OBJECTIVES ON UNETR PERFORMANCE

Weight Initialization	Spleen	R.kidney	L.kidney	G.bladder	Liver	Stomach	Aorta	Pancreas	Average
Default [7]	88.58	80.03	78.87	62.51	95.45	74.44	84.79	52.70	77.17
masking [37]	85.75	82.26	84.50	59.84	95.61	72.37	88.14	60.17	78.58
Tube masking [38]	87.54	82.48	83.90	58.66	95.36	73.48	86.55	58.25	78.28
Order prediction (Ours)	88.22	83.42	85.03	62.08	95.36	70.56	86.86	60.24	78.97
Order prediction + masking (Ours)	86.72	82.86	85.41	65.15	95.56	75.23	88.07	58.85	79.73

TABLE VII
EFFICIENCY IN TERMS OF TOTAL TRAINING EPOCHS

Method	UNETR		UNETR (Ours)	
Epochs	5000	5800	800+4200	800+5000
Dice (%)	77.17	77.46	79.20	79.73

TABLE VIII
EFFECT OF INTERMEDIATE ENCODER REPRESENTATIONS

Classifier	Dice (%)
t4	77.87
t3 + t4	78.60
t2 + t3 + t4	79.10
t1+t2+t3+t4 (Ours)	79.73

of different self-supervised objectives on UNETR performance is discussed in Table VI. Our proposed combination of multi-objective self supervised tasks performs better than existing masking based self-supervised pretraining approaches [37], [38] and shuffling order prediction alone. These results demonstrate that our approach combines the advantages of both masked image reconstruction and shuffled order prediction effectively by capturing structural as well as contextual consistencies in the available training data.

Effect of intermediate encoder representations: We studied the effect of utilizing intermediate encoder representations for order prediction during the initialization step (step-1) and the results are shown in Table VIII. Here, t_i represents the order predictions generated using intermediate encoder representation at layer i . We observe that incorporating the order predictions from multiple resolutions to capture details at various levels of granularity for accurately delineating boundaries and capturing fine-grained details and thereby improves the overall segmentation performance of UNETR.

Comparison with Swin-UNETR large scale pretraining: We compared our proposed initialization approach against the self-supervised pretraining framework introduced in [10] which involves pretraining Swin-UNETR encoder using a cohort of 5050 CT images on multi-objective self supervised tasks to learn robust feature representations to improve downstream segmentation. By incorporating our proposed weight initialization approach which utilizes the available training

TABLE IX
SWIN-UNETR SINGLE MODEL RESULTS

Method	Pretrained	Synapse	BTCV
Swin-UNETR [1]	×	79.71	80.51
Swin-UNETR [10]	✓	81.08	81.59
Swin-UNETR (Ours)	×	81.41	81.36

data only, we could achieve promising results comparable to the single model results of pretrained Swin-UNETR model in terms of average dice score. The results for Swin-UNETR multi-organ segmentation datasets BTCV and Synapse are demonstrated in Table IX.

V. CONCLUSION

In this work, we introduce a data-dependent weight initialization scheme that is designed to capture the volumetric data characteristics effectively in order to improve the downstream segmentation task. We propose to first train the model on tailored multi-objective self-supervised tasks to learn the contextual and structural consistency from the limited training data. The trained model weights will then be utilized to initialize the supervised training for segmentation. We demonstrate that our approach is complementary and can be easily integrated into any hybrid segmentation model to improve performance.

REFERENCES

- [1] A. Hatamizadeh, V. Nath, Y. Tang, D. Yang, H. R. Roth, and D. Xu, "Swin unetr: Swin transformers for semantic segmentation of brain tumors in mri images," in *International MICCAI Brainlesion Workshop*, pp. 272–284, Springer, 2021.
- [2] H. Cao, Y. Wang, J. Chen, D. Jiang, X. Zhang, Q. Tian, and M. Wang, "Swin-unet: Unet-like pure transformer for medical image segmentation," in *European conference on computer vision*, pp. 205–218, Springer, 2022.
- [3] Z. Zhou, V. Sodha, J. Pang, M. B. Gotway, and J. Liang, "Models genesis," *Medical image analysis*, vol. 67, p. 101840, 2021.
- [4] A. Dosovitskiy, L. Beyer, A. Kolesnikov, D. Weissenborn, X. Zhai, T. Unterthiner, M. Dehghani, M. Minderer, G. Heigold, S. Gelly, *et al.*, "An image is worth 16x16 words: Transformers for image recognition at scale," *arXiv preprint arXiv:2010.11929*, 2020.
- [5] A. Vaswani, N. Shazeer, N. Parmar, J. Uszkoreit, L. Jones, A. N. Gomez, L. Kaiser, and I. Polosukhin, "Attention is all you need," *Advances in neural information processing systems*, vol. 30, 2017.
- [6] S. Khan, M. Naseer, M. Hayat, S. W. Zamir, F. S. Khan, and M. Shah, "Transformers in vision: A survey," *ACM computing surveys (CSUR)*, vol. 54, no. 10s, pp. 1–41, 2022.

- [7] A. Hatamizadeh, Y. Tang, V. Nath, D. Yang, A. Myronenko, B. Landman, H. R. Roth, and D. Xu, "Unetr: Transformers for 3d medical image segmentation," in *Proceedings of the IEEE/CVF winter conference on applications of computer vision*, pp. 574–584, 2022.
- [8] X. Glorot and Y. Bengio, "Understanding the difficulty of training deep feedforward neural networks," in *Proceedings of the thirteenth international conference on artificial intelligence and statistics*, pp. 249–256, JMLR Workshop and Conference Proceedings, 2010.
- [9] K. He, X. Zhang, S. Ren, and J. Sun, "Delving deep into rectifiers: Surpassing human-level performance on imagenet classification," in *Proceedings of the IEEE international conference on computer vision*, pp. 1026–1034, 2015.
- [10] Y. Tang, D. Yang, W. Li, H. R. Roth, B. Landman, D. Xu, V. Nath, and A. Hatamizadeh, "Self-supervised pre-training of swin transformers for 3d medical image analysis," in *Proceedings of the IEEE/CVF Conference on Computer Vision and Pattern Recognition*, pp. 20730–20740, 2022.
- [11] J. Long, E. Shelhamer, and T. Darrell, "Fully convolutional networks for semantic segmentation," in *Proceedings of the IEEE conference on computer vision and pattern recognition*, pp. 3431–3440, 2015.
- [12] L.-C. Chen, G. Papandreou, I. Kokkinos, K. Murphy, and A. L. Yuille, "DeepLab: Semantic image segmentation with deep convolutional nets, atrous convolution, and fully connected crfs," *IEEE transactions on pattern analysis and machine intelligence*, vol. 40, no. 4, pp. 834–848, 2017.
- [13] O. Ronneberger, P. Fischer, and T. Brox, "U-net: Convolutional networks for biomedical image segmentation," in *Medical Image Computing and Computer-Assisted Intervention–MICCAI 2015: 18th International Conference, Munich, Germany, October 5–9, 2015, Proceedings, Part III 18*, pp. 234–241, Springer, 2015.
- [14] Q. Dou, H. Chen, Y. Jin, L. Yu, J. Qin, and P.-A. Heng, "3d deeply supervised network for automatic liver segmentation from ct volumes," in *Medical Image Computing and Computer-Assisted Intervention–MICCAI 2016: 19th International Conference, Athens, Greece, October 17–21, 2016, Proceedings, Part II 19*, pp. 149–157, Springer, 2016.
- [15] L. Yu, X. Yang, H. Chen, J. Qin, and P. A. Heng, "Volumetric convnets with mixed residual connections for automated prostate segmentation from 3d mr images," in *Proceedings of the AAAI Conference on Artificial Intelligence*, vol. 31, 2017.
- [16] X. Li, H. Chen, X. Qi, Q. Dou, C.-W. Fu, and P.-A. Heng, "H-denseunet: hybrid densely connected unet for liver and tumor segmentation from ct volumes," *IEEE transactions on medical imaging*, vol. 37, no. 12, pp. 2663–2674, 2018.
- [17] Q. Zhu, B. Du, B. Turkbey, P. L. Choyke, and P. Yan, "Deeply-supervised cnn for prostate segmentation," in *2017 international joint conference on neural networks (IJCNN)*, pp. 178–184, IEEE, 2017.
- [18] E. Gibson, F. Giganti, Y. Hu, E. Bonmati, S. Bandula, K. Gurusamy, B. Davidson, S. P. Pereira, M. J. Clarkson, and D. C. Barratt, "Automatic multi-organ segmentation on abdominal ct with dense v-networks," *IEEE transactions on medical imaging*, vol. 37, no. 8, pp. 1822–1834, 2018.
- [19] F. Milletari, N. Navab, and S.-A. Ahmadi, "V-net: Fully convolutional neural networks for volumetric medical image segmentation," in *2016 fourth international conference on 3D vision (3DV)*, pp. 565–571, Ieee, 2016.
- [20] Ö. Çiçek, A. Abdulkadir, S. S. Lienkamp, T. Brox, and O. Ronneberger, "3d u-net: learning dense volumetric segmentation from sparse annotation," in *Medical Image Computing and Computer-Assisted Intervention–MICCAI 2016: 19th International Conference, Athens, Greece, October 17–21, 2016, Proceedings, Part II 19*, pp. 424–432, Springer, 2016.
- [21] F. Isensee, P. F. Jaeger, S. A. Kohl, J. Petersen, and K. H. Maier-Hein, "nnu-net: a self-configuring method for deep learning-based biomedical image segmentation," *Nature methods*, vol. 18, no. 2, pp. 203–211, 2021.
- [22] H. R. Roth, H. Oda, Y. Hayashi, M. Oda, N. Shimizu, M. Fujiwara, K. Misawa, and K. Mori, "Hierarchical 3d fully convolutional networks for multi-organ segmentation," *arXiv preprint arXiv:1704.06382*, 2017.
- [23] D. Karimi, S. D. Vasylechko, and A. Gholipour, "Convolution-free medical image segmentation using transformers," in *Medical Image Computing and Computer Assisted Intervention–MICCAI 2021: 24th International Conference, Strasbourg, France, September 27–October 1, 2021, Proceedings, Part I 24*, pp. 78–88, Springer, 2021.
- [24] J. Chen, Y. Lu, Q. Yu, X. Luo, E. Adeli, Y. Wang, L. Lu, A. L. Yuille, and Y. Zhou, "Transunet: Transformers make strong encoders for medical image segmentation," *arXiv preprint arXiv:2102.04306*, 2021.
- [25] A. Lin, B. Chen, J. Xu, Z. Zhang, G. Lu, and D. Zhang, "Ds-transunet: Dual swin transformer u-net for medical image segmentation," *IEEE Transactions on Instrumentation and Measurement*, vol. 71, pp. 1–15, 2022.
- [26] Y. Zhang, H. Liu, and Q. Hu, "Transfuse: Fusing transformers and cnns for medical image segmentation," in *Medical Image Computing and Computer Assisted Intervention–MICCAI 2021: 24th International Conference, Strasbourg, France, September 27–October 1, 2021, Proceedings, Part I 24*, pp. 14–24, Springer, 2021.
- [27] J. M. J. Valanarasu, P. Oza, I. Hacihaliloglu, and V. M. Patel, "Medical transformer: Gated axial-attention for medical image segmentation," in *Medical Image Computing and Computer Assisted Intervention–MICCAI 2021: 24th International Conference, Strasbourg, France, September 27–October 1, 2021, Proceedings, Part I 24*, pp. 36–46, Springer, 2021.
- [28] A. Shaker, M. Maaz, H. Rasheed, S. Khan, M.-H. Yang, and F. S. Khan, "Unetr++: Delving into efficient and accurate 3d medical image segmentation," *arXiv preprint arXiv:2212.04497*, 2022.
- [29] H.-Y. Zhou, J. Guo, Y. Zhang, L. Yu, L. Wang, and Y. Yu, "nnformer: Interleaved transformer for volumetric segmentation," *arXiv preprint arXiv:2109.03201*, 2021.
- [30] W. Wang, C. Chen, M. Ding, H. Yu, S. Zha, and J. Li, "Transbts: Multimodal brain tumor segmentation using transformer," in *Medical Image Computing and Computer Assisted Intervention–MICCAI 2021: 24th International Conference, Strasbourg, France, September 27–October 1, 2021, Proceedings, Part I 24*, pp. 109–119, Springer, 2021.
- [31] Z. Liu, Y. Lin, Y. Cao, H. Hu, Y. Wei, Z. Zhang, S. Lin, and B. Guo, "Swin transformer: Hierarchical vision transformer using shifted windows," in *Proceedings of the IEEE/CVF international conference on computer vision*, pp. 10012–10022, 2021.
- [32] H. Li, Z. Xu, G. Taylor, C. Studer, and T. Goldstein, "Visualizing the loss landscape of neural nets," *Advances in neural information processing systems*, vol. 31, 2018.
- [33] A. Hatamizadeh, Z. Xu, D. Yang, W. Li, H. Roth, and D. Xu, "Unet-former: A unified vision transformer model and pre-training framework for 3d medical image segmentation," *arXiv preprint arXiv:2204.00631*, 2022.
- [34] X. Huang, Z. Deng, D. Li, and X. Yuan, "Missformer: An effective medical image segmentation transformer," *arXiv preprint arXiv:2109.07162*, 2021.
- [35] B. Landman, Z. Xu, J. Igelsias, M. Styner, T. Langerak, and A. Klein, "Miccai multi-atlas labeling beyond the cranial vault—workshop and challenge," in *Proc. MICCAI Multi-Atlas Labeling Beyond Cranial Vault—Workshop Challenge*, vol. 5, p. 12, 2015.
- [36] A. L. Simpson, M. Antonelli, S. Bakas, M. Bilello, K. Farahani, B. Van Ginneken, A. Kopp-Schneider, B. A. Landman, G. Litjens, B. Menze, *et al.*, "A large annotated medical image dataset for the development and evaluation of segmentation algorithms," *arXiv preprint arXiv:1902.09063*, 2019.
- [37] K. He, X. Chen, S. Xie, Y. Li, P. Dollár, and R. Girshick, "Masked autoencoders are scalable vision learners," in *Proceedings of the IEEE/CVF Conference on Computer Vision and Pattern Recognition*, pp. 16000–16009, 2022.
- [38] C. Feichtenhofer, Y. Li, K. He, *et al.*, "Masked autoencoders as spatiotemporal learners," *Advances in neural information processing systems*, vol. 35, pp. 35946–35958, 2022.